Astron. & Astrophys. 25, 415–430 (1973)

Interpretation of Hydrogen Lyman-Alpha Observations of Comets Bennett and Encke

J. L. Bertaux, J. E. Blamont and M. Festou

Service d'Aéronomie du C.N.R.S.
Verrières-le-Buisson, France

Received February 8, revised March 15, 1973

Summary. The Lyman-Alpha emission of the hydrogen cloud surrounding comet Bennett was mapped from the OGO–5 satellite observations during the whole month of April 1970. The measured distribution of intensity was compared to a theoretical model of hydrogen cloud in which atoms leave radially the cometary head with a maxwellian velocity distribution. They are then influenced by the solar Lyman-Alpha (Ly α) radiation pressure, photoionization by solar EUV and charge exchange with solar wind protons. The production rate of hydrogen atoms measured by the number of hydrogen atoms Q_W emitted per second and per steradian, the ejection velocity v_W and the lifetime τ_H of the hydrogen atom before ionization which are the parameters of the model were adjusted to the twelve maps obtained, when the sun-comet distance R increased from 0.6 Astronomical Units to 1.04 AU.

The ejection rate Q_W was found to follow approximately a R^{-2} law, with a value of 0.7×10^{29} atom $\cdot$ sterad^{-1}s^{-1} at 0.81 AU. The ejection velocity remained nearly constant at 8 ± 2 km s^{-1}. This value is compatible with a pure water model, if the photodissociation of OH produces atoms with a velocity distribution peaked at 8 km s^{-1} at least, a condition which is not in contradiction with what is known about the OH photodissociation.

The data suggested also that the lifetime of H atoms would be shorter outside the ecliptic plane, which could be explained by an increase in the charge exchange efficiency by a factor of 3 for heliographic latitudes larger than 45°.

The ejection rate of H atoms in comet Encke was estimated to be $\simeq 5 \times 10^{26}$ atom $\cdot$ sterad^{-1} s^{-1}.

Key words: comets – hydrogen – Lyman-Alpha

Introduction

A strong Lyman-Alpha emission has been recently observed in three comets, as a result of resonant scattering of solar Lyman-Alpha radiation by neutral hydrogen produced in their comas. Such a feature in the ultraviolet emission cometary spectrum had been predicted by Biermann (Biermann and Trefftz, 1964; Biermann, 1968) and the first Lyman-Alpha observation of the head of comet TAGO SATO KOSAKA (1969g) by OAO–2, was a brilliant confirmation of the predicted feature (Code *et al.*, 1970). This comet was also observed from an Aerobee rocket in January, 1970 (Jenkins and Wingert, 1972); the recorded Lyman-Alpha image was 8×10^5 km in diameter.

Comet Bennett (1969i) was first observed in Lyman-Alpha by Bertaux and Blamont (1970) and later from OAO–2 (Code *et al.*, 1970) and from the other Lyman-Alpha photometer on board OGO–5 (Thomas, 1973). The extent of the emissive region observed by the Bertaux and Blamont photometer was $\simeq 15 \times 10^6$ km, much larger than the observed emissive region with the OAO–2 instrument, 3×10^6 km in diameter, owing to the greater field of view and sensitivity of the OGO–5 instrument. The Lyman-Alpha emission of comet Bennett was monitored during the whole month of April, 1970, with this instrument. For this purpose, we requested that the OGO–5 spacecraft be put in a slow spin motion with its spin axis along the sun-spacecraft line and a period of approximately 30 minutes. From April 1–30, 1970, twelve maps of the Lyman-Alpha emission were obtained with a resolution of 0.7°.

Though much fainter than comet Bennett, the periodic comet Encke (1970e) was observed in December, 1970, with the same instrument.

The purpose of this paper is to present these observations of comets Bennett and Encke, and an analysis of the results, based on a comparison of the observed intensity maps with a theoretical model of the cometary hydrogen cloud. The production (or ejection) rate of atomic hydrogen, the ejection velocity and the lifetime of the produced atoms were determined, as well as their variations during one month. From their absolute values and their variations some information can be

derived concerning the number density and the nature of the "parent molecules" of the type MH before photodissociation (M means an unknown radical).

In the outer regions of the cometary coma ($r > 10^5$ km) the hydrogen atmosphere expands out radially with a mean velocity v_H. In a simple model the atomic hydrogen distribution follows a r^{-2} law and the intensity a r^{-1} law. These distributions are in this case only a function of the ratio $\frac{Q_t}{v_H}$ where Q_t is the total production rate of hydrogen atoms. However, the real case departs from this simple model because of two different effects. First, the Lyman-Alpha radiation pressure is not negligible as compared to the solar attraction, and the trajectories can no longer be considered as straight lines emerging from the nucleus. Second, an H-atom can be ionized either by the EUV solar flux with $\lambda < 912$ Å, or by charge exchange with the protons of the solar wind. They have thus a limited lifetime τ_H.

If these two effects can be neglected in the central region of the coma ($r < 10^6$ km) observed from OAO–2, they are of primary importance in the outer region ($r > 10^6$ km) observed with our instrument on OGO–5. In this region, called the cometary hydrogen envelope, the atomic hydrogen density (and consequently the Lyman-Alpha intensity distribution) is controlled by the interaction between the flow of hydrogen atoms and the solar phenomena. One would then expect that observations of the outer hydrogen cloud which is optically thin will provide information about both the hydrogen outflow and its interactive environment; in particular, as comet Bennett was observed at ecliptic latitudes up to 80°, we tried to detect a variation of the lifetime τ_H with ecliptic latitude, owing to a possible variation of the solar wind intensity.

In the following section we describe the experimental procedure of the data collection and the construction of emission maps. In a later section, the physical assumptions for the theoretical model are presented. The comparison of computed Lyman-Alpha intensity with measurements provides the parameters of the hydrogen flow and their variations during the month of April, 1970. A discussion follows on the physical implications of the results, concerning the number and the nature of the "parent molecules". An intensity map of comet Encke is also presented.

Data Collection and Map Construction

The instrument of Service d'Aéronomie on board OGO–5 has been previously described (Bertaux and Blamont, 1970). It is essentially a photometer with a 40′ field of view, a 80 Å bandwidth centered at Lyman-Alpha (1216 Å), and a step by step scanning mirror. Its primary objective was to determine the hydrogen density distribution in the geocorona through the mapping of emerging Lyman-Alpha intensity. A hydrogen cell, associated with the instrument in order to measure the linewidth of the Lyman-Alpha emission, was unfortunately not operative during the comet Bennett observations.

OGO–5 was launched on March 4, 1968, on a very eccentric orbit, with an apogee of 153000 km. In its normal operation it was three axis stabilized. However, special de-stabilization operations were performed to map the extra-geocoronal Lyman-Alpha intensity on several occasions since September, 1969, at three months intervals. This mapping revealed that the extra-geocoronal Lyman-Alpha emission was the result of resonant scattering of the solar Lyman-Alpha by the hydrogen atoms of the interstellar medium penetrating the solar system.

The third operation of this kind began on April 1, 1970, and during this operation the Lyman-Alpha emission of comet Bennett was discovered. The observation of the Lyman-Alpha emission of comet Bennett was successful enough to justify leaving the spacecraft in the spinning mode to monitor the evolution of its hydrogen cloud. This monitoring was authorized by NASA Headquarters, and twelve maps of Lyman-Alpha emission were obtained from April 1 to 30, 1970.

During the whole month, the spacecraft was left in a slow spin motion about the solar direction, with a period of approximately 30 minutes. The scanning mirror of the instrument could be fixed in a given position, the field of view axis describing a cone about the spin axis. The apex angle of this cone (or solar elongation) was controlled by moving the mirror on ground command in steps of 0.5°. The operations required to obtain enough data to establish one map were made when the spacecraft was at apogee to avoid contamination of the data by geocoronal Lyman-Alpha.

The geometry of the orbit of comet Bennett is illustrated in Fig. 1. The sun-comet distance was 0.606 AU and the earth-comet distance was 0.72 AU on April 1. On April 30, these distances were, respectively, 1.04 AU and 1.33 AU. The orbital plane of comet Bennett was crossed by the earth on May 4, 1970; its inclination on the ecliptic plane was 90°. This means that the earth was never far away from the orbital plane during the whole month of April, making it difficult to detect a curvature of the cometary hydrogen cloud in the orbital plane. At each rotation of the spacecraft, the field of view of the instrument crossed the cometary cloud along a line perpendicular to the projection of the sun-comet line on the celestial sphere. The cloud emission was identified on the recorded data as a large bump superimposed on the $\simeq 300$ Rayleigh of interplanetary Lyman-Alpha background (Fig. 2). In order to reconstruct a map of the emission of the whole cloud, it was assumed that all the profiles obtained with different apex angles had their maxima aligned with the projection of the sun-comet vector on the celestial sphere. The distribution along such a line of the intensity maxima of each perpendicular profile is presented on Figs. 3–5 as a function of solar

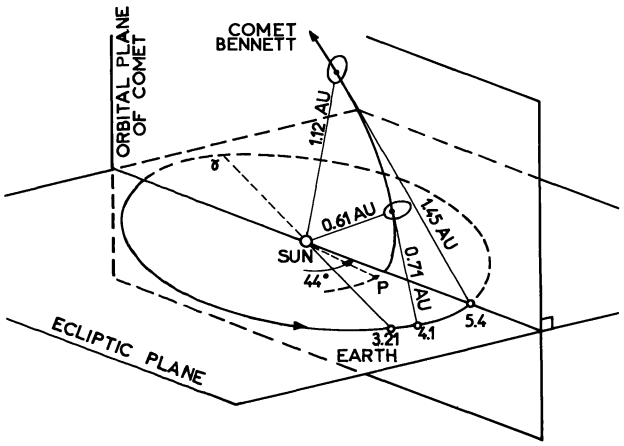

Fig. 1. The inclination of the orbital plane of comet Bennett (1969 i) on the ecliptic plane was 90°. The relative positions of the earth and the comet are indicated for April 4, 1970 and May 4, 1970, covering the whole period of OGO-5 observations. The comet crossed the ecliptic plane shortly after perihelion and was at 1.11 AU above it on May 4, 1970, when the earth crossed its orbital plane

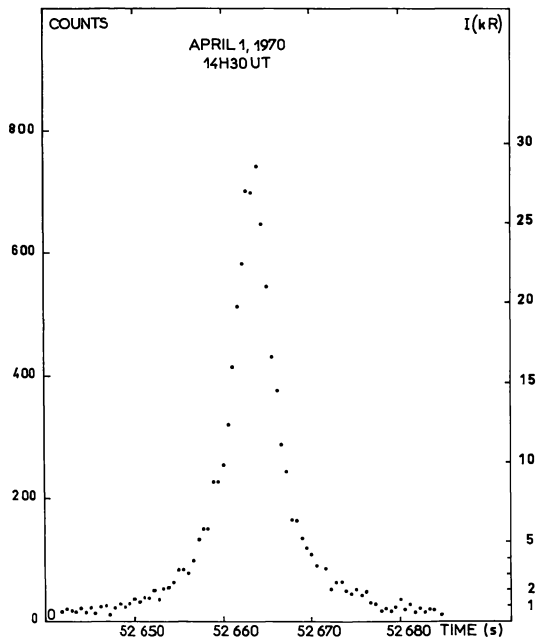

Fig. 2. The data points of one profile are plotted in number of counts as a function of time during one rotation of the spacecraft. The corresponding Lyman-Alpha intensity is indicated on the right. The maximum intensity was 28 kilo Rayleigh for this profile

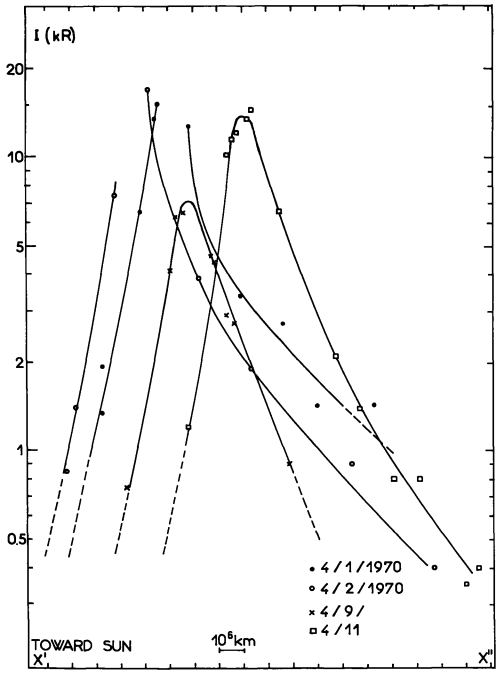

Fig. 3

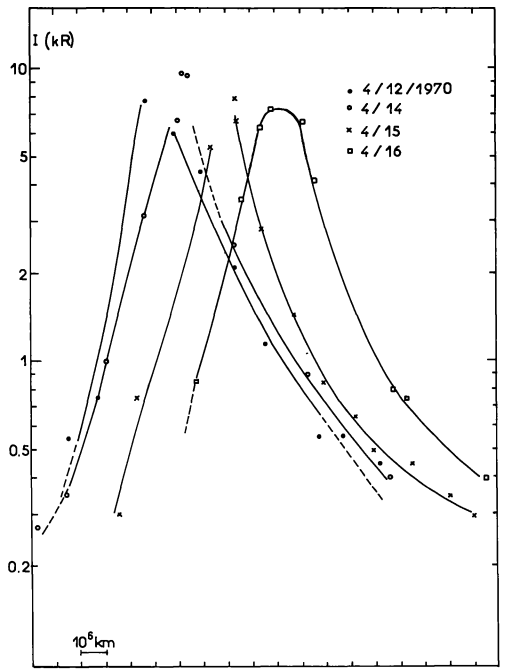

Fig. 4

Figs. 3–5. The distributions of intensity maxima along the sun-comet vector as a function of distance projected on the celestial sphere are indicated for the twelve maps. As the position of the nucleus is not well known, relative positions of distributions are arbitrary along the $X'X''$ axis

elongation of the profile. This distribution is peaked at a point which should not be far away from the nucleus. In the following we call forward profile and backward profile the parts of this distribution located respectively on the same side as the sun or on the opposite side in respect to the nucleus (Fig. 6). Though there remains some uncertainty on the solar elongation of the profiles relative to the solar elongation of the nucleus as predicted by the ephemeris, it is felt that the location of each profile relative to the others is known with an accuracy better than 0.2°.

It was also assumed that the angular velocity of the spacecraft was constant during one rotation. Each time a bright star could be seen near the comet, it has been possible to check the validity of this last assumption with an accuracy better than 10%.

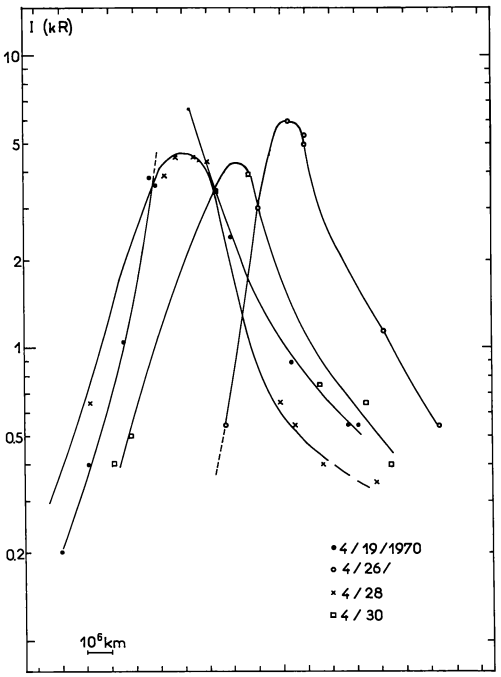

Fig. 5

The map established from the profiles observed on April 1, 1970 is presented in Fig. 6 under the form of iso-intensity contours. The error bars for this map are typical of all the maps presented in Figs. 6–17. On April 1, 1970, the size of the hydrogen envelope where the emission was larger than 250 Rayleigh was 20×10^6 km along the sun-comet vector and 15×10^6 km perpendicularly. The brightest emission recorded in the 40′ field of view of the instrument was 28 kilo Rayleigh. However the intensity gradient around the nucleus was so large that the true central intensity was certainly higher. Later on, though the general shape of the isophotes was approximately maintained, the emission decreased as the comet was going away from the sun.

The map obtained on April 9, 1970, is not complete and seems to be slightly different from the other maps; the central isophotes seems to be more compressed along the sun-comet vector, though their perpendicular size are similar to the corresponding ones of adjacent maps. This map was obtained with exactly the same procedure as the other ones and up to now we could not think of any experimental effect which could have induced this feature.

The three last maps obtained on April 26, 28 and 30, 1970 seem to be more elongated than the other ones in the perpendicular direction (as they were found to be symmetrical, only one-half was represented). These maps should be considered with caution, because the earth-comet distance was slightly larger than for the precedings ones increasing the portion of comet in the 40′ field of view. Furthermore, the spin rate of the spacecraft was doubled just before April 26; though this change of spin rate was included in the data reduction, it is not

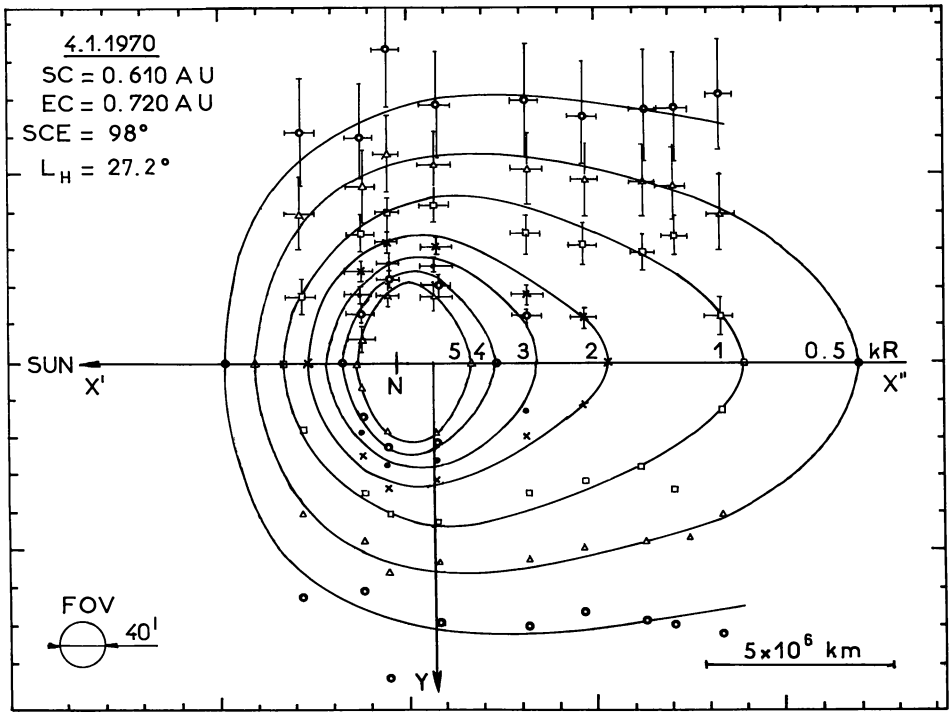

Fig. 6. Lyman-Alpha isophotes of comet Bennett as observed April 1, 1970 from 0.5 to 5 kilo Rayleigh. The 300 Rayleigh Lyman-Alpha background was substracted from all measurements. The 40′ diameter of the field-of-view (circle) represented approximately 10^6 km at the distance EC of the comet. The sun-comet distance SC was 0.61 AU, the sun-comet-earth angle SCE was 98° and the heliographic latitude L_H was 27.2°. The intensity distribution along the sun vector $X'X''$ and perpendicular to it (in a plane located 10^6 km behind the nucleus N) were compared to a theoretical model

completely impossible that it could have introduced unknown irregularities in the angular velocity of the spacecraft. Such an effect might be responsible for the different aspect of the last three maps.

In order to interpret the emission pattern and its variations, a theoretical model of the hydrogen envelope surrounding a comet was constructed, and the corresponding Lyman-Alpha emission was computed as it is now described.

The Hydrogen Envelope Model

This model is derived from the "fountain model" proposed by Haser (1965). It describes the distribution of hydrogen atoms in the outer region of the hydrogen clouds, where collisions become negligible. The atoms emerge radially from the nucleus (or a small region around the nucleus of radius r_A) and their individual trajectories in the solar system are determined by the combination of two central forces having opposite

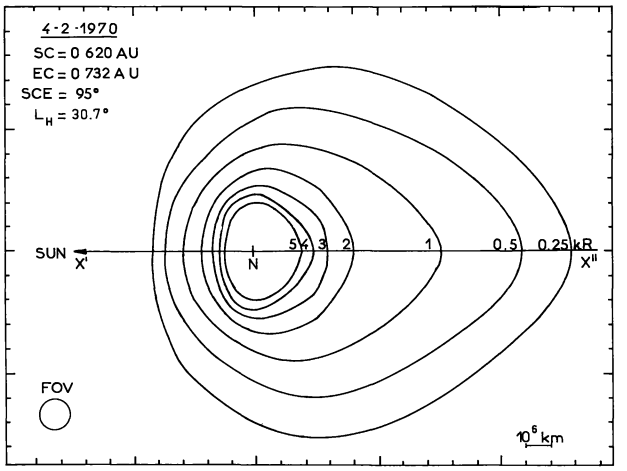

Fig. 7

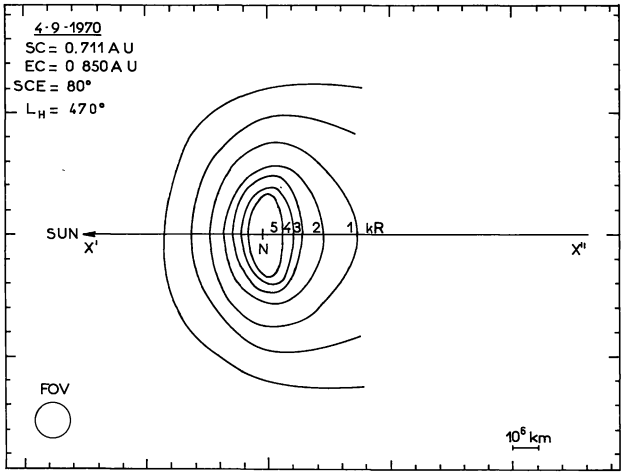

Fig. 8

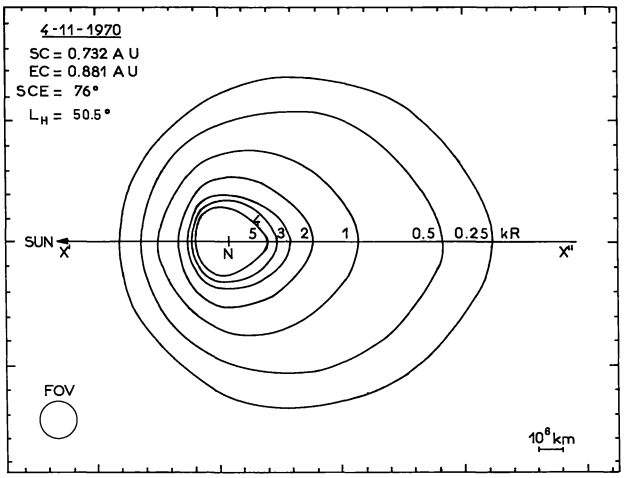

Fig. 9

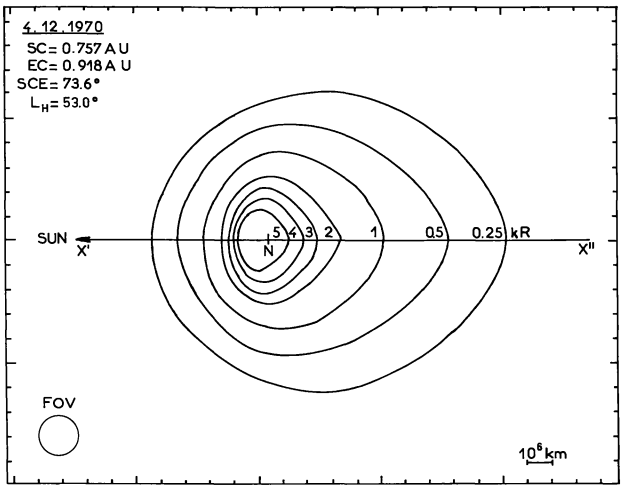

Fig. 10

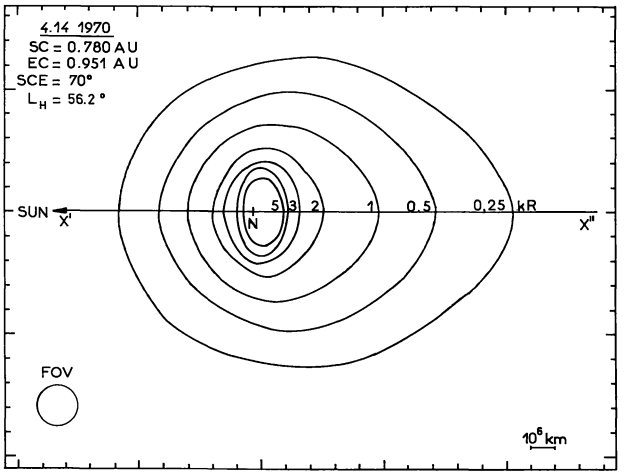

Fig. 11

Figs. 7 – 17. Evolution of the Lyman-Alpha isophotes along the month of April, 1970. The conditions of observation are indicated in the upper left of each map. As the distance earth-comet EC increased, the field of view FOV of the photometer subtended larger areas of the comet, and the accuracy was somewhat poorer for the three last maps

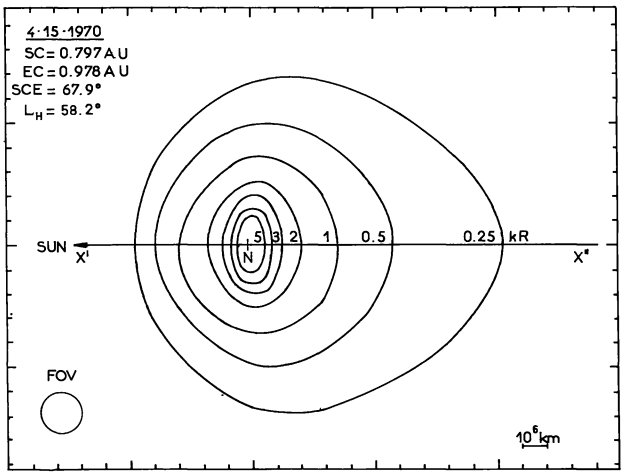

Fig. 12

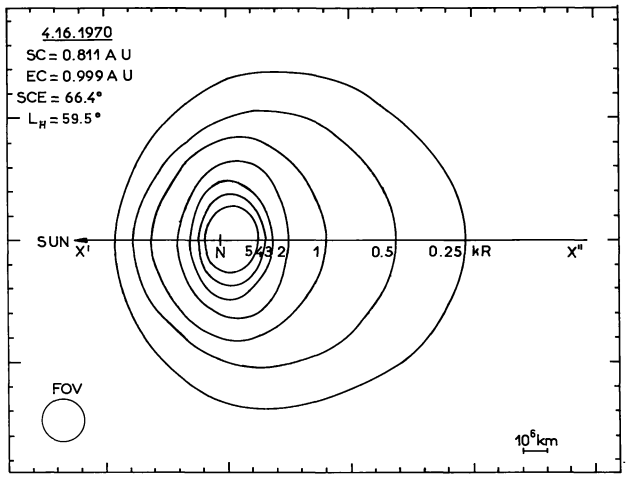

Fig. 13

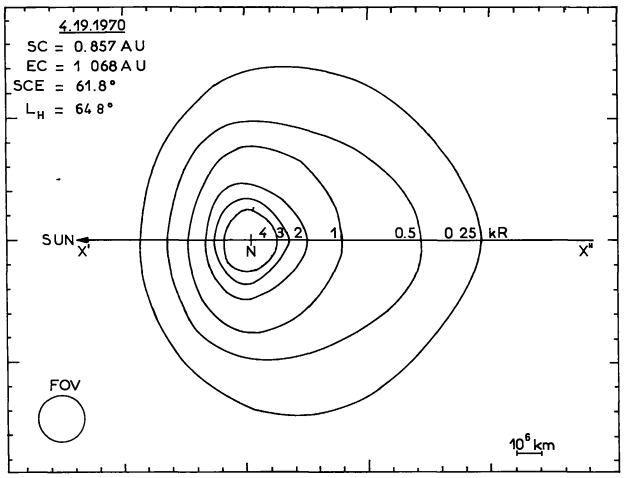

Fig. 14

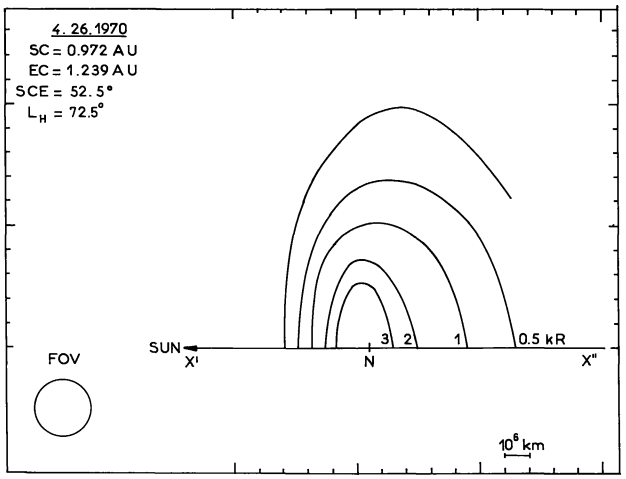

Fig. 15

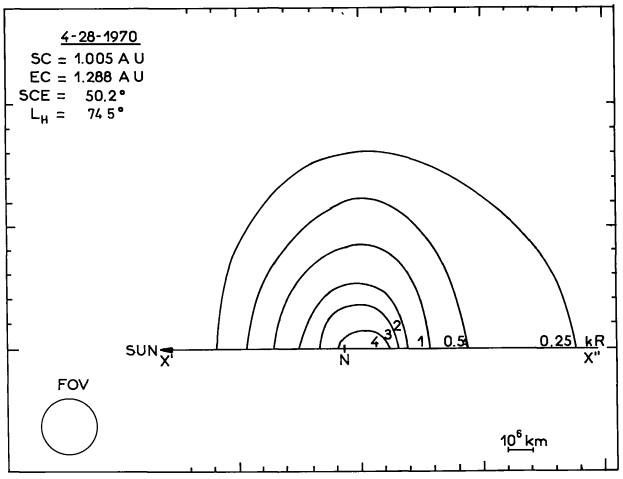

Fig. 16

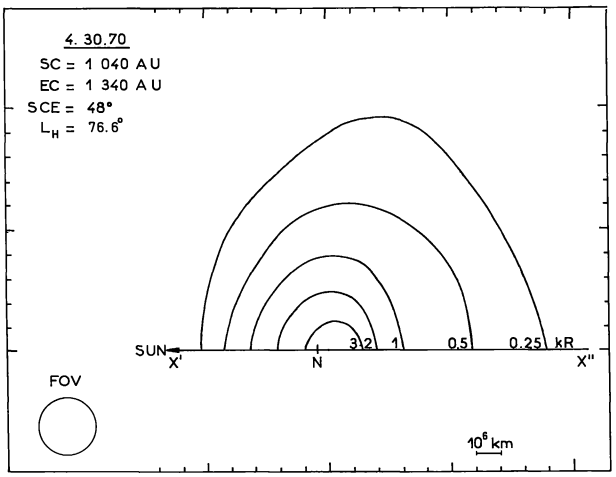

Fig. 17

directions: γ_s, due to the solar gravitation and γ, due to the Lyman-Alpha radiation pressure. Both forces follow a R^{-2} power law (R is the sun-comet distance). At 1 AU their values are, respectively, 0.59 cm s^{-2} and 0.82 cm s^{-2}, for a Lyman-Alpha solar flux of 4.6×10^{11} photon/cm^2 Å s (Vidal Madjar *et al.*, 1973).

The trajectory of a hydrogen atom can be described in a system of reference attached to the nucleus N whose axis NX is directed towards the sun (Fig. 18). In the neighborhood of the nucleus, the trajectory is a parabola contained in a meridian plane (NX, NY) if the Coriolis acceleration is neglected, since the H-atom is submitted to the constant acceleration γ in the anti-solar direction.

We assume that the ejection rate Q_W is isotropic and is then related to the total production rate of hydrogen atoms Q_t by $Q_W = Q_t/4\pi$. Consequently, the distribution of hydrogen atoms inside the cometary envelope has a cylindrical symmetry about the sun-comet vector.

From April 1–30, the comet heliocentric distance R increased from 0.606 AU to 1.04 AU. As the variation of R during the lifetime of one atom is not negligible, atoms which are observed at the time t had been emitted at the time $t - \Delta t$ from the nucleus when it was nearer to the sun. The production rate $Q_W(t)$ being probably smaller than $Q_W(t - \Delta t)$ it was assumed that between $t - \Delta t$ and t, Q_W had followed a R^{-2} power law. This assumption will be *a posteriori* approximately verified.

The hydrogen atoms are ionized by charge-exchange with the solar wind protons and by photo-ionization from the EUV solar flux with $\lambda < 912$ Å. The lifetime τ_H of an H-atom can be expressed as a function of the photo-ionization rate J, the charge-exchange cross section σ_{ex}, and the flux of solar protons ϕ_p:

$$\tau_H = \frac{1}{J + \sigma_{ex}\phi_p} \tag{1}$$

Monocinetic Model

We first consider a monocinetic model in which all the particles have the same radial ejection velocity v. In such a model, the density distribution can be described as a function $n(r,\theta,v)$ of the parameter v and of the point P of coordinates r,θ (r is the radial distance and θ the angle between the sun vector and the direction of the point). We shall first consider the density $n^*(r,\theta,v)$ for the case of a hydrogen atom with an infinite lifetime. At any point P of coordinates r,θ, there are two parabolae emerging from the nucleus with the velocity v (Fig. 18), at angles α_1 and α_2, respectively, with the comet-sun vector. Then the density at the point r,θ is the sum of two densities corresponding to each value of α:

$$n^*(r,\theta,v) = n^*_{\alpha_1}(r,\theta,v) + n^*_{\alpha_2}(r,\theta,v). \tag{2}$$

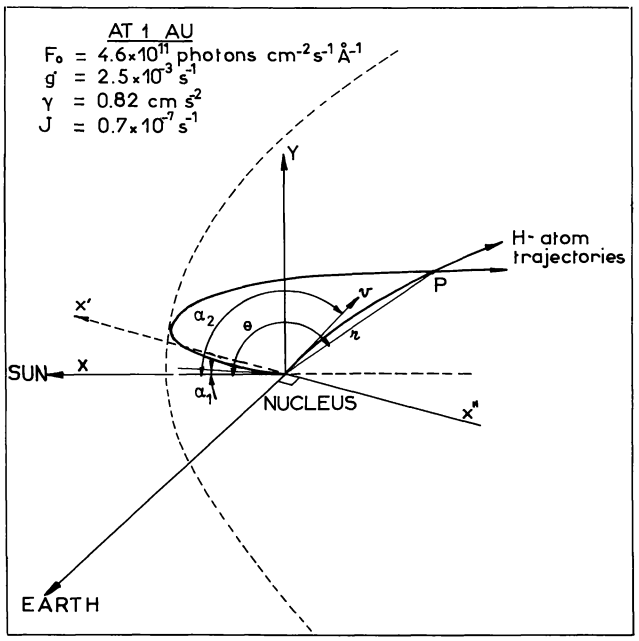

Fig. 18. In the theoretical model of cometary envelope the trajectories of H-atoms coming out radially from the nucleus with a given velocity v are bent into parabolae by the Lyman-Alpha radiation pressure, in a coordinates system attached to the nucleus. The trajectories are contained inside a paraboloid (dotted line). At any given point P inside the paraboloid there are two different trajectories indicated in the XY plane in the figure. Physical constants at 1 AU taken for the computations are indicated: Lyman-Alpha solar flux F_0, excitation rate g, acceleration γ, photo-ionization rate of a H-atom

For a point r,θ, the two values of α are expressed by:

$$\alpha_{1,2} = \frac{\theta}{2} \mp \frac{1}{2} \arccos\left[\frac{1}{r}\left(x + \frac{\gamma y^2}{v}\right)\right] \tag{3}$$

in which $x = r\cos\theta$ and $y = r\sin\theta$ are the cartesian coordinates of P.

The density corresponding to a specific value of α can be computed by taking the flux of the particles between the two parabolae α and $\alpha + d\alpha$ to be conservative all along the parabolae. We find after computations that the density for a specific value of α is:

$$n^*_\alpha(r,\theta,v) = \frac{Q_W}{y^2} \cdot \frac{v\sin^3\alpha}{\gamma y\cos\alpha - v^2\sin\alpha}. \tag{4}$$

The effective density $n_\alpha(r,\theta,v)$ is equal to the density $n^*_\alpha(r,\theta,v)$ multiplied by the extinction factor:

$$n_\alpha(r,\theta,v) = n^*_\alpha(r,\theta,v)\exp\left(-\int_0^t \frac{dt}{\tau_H(t)}\right) \tag{5}$$

where $t = \dfrac{y}{v\sin\alpha}$ is the time a hydrogen atom takes to describe its trajectory up to its position r,θ. Assuming

that the lifetime τ_H is constant along the trajectories, the total density at the point r,θ is then:

$$n(r,\theta,v) = n^*_{\alpha_1}(r,\theta,v)\exp\left(\frac{-y}{v\sin\alpha_1\tau_H}\right) + n^*_{\alpha_2}(r,\theta,v)\exp\left(\frac{-y}{v\sin\alpha_2\tau_H}\right). \quad (6)$$

Combining Eqs. (3) and (6) the density at the point r,θ in a monocinetic model is:

$$n(r,\theta,v) = Q_W(\phi_{\alpha_1}(r,\theta,v) + \phi_{\alpha_2}(r,\theta,v)) \quad (7)$$

where the function $\phi_\alpha(r,\theta,v)$ is:

$$\phi_\alpha(r,\theta,v) = \frac{1}{y^2}\frac{v\sin^3\alpha}{\gamma y\cos\alpha - v^2\sin\alpha}\exp\left(-\frac{y}{v\sin\alpha\tau_H}\right)$$

In such a monocinetic model all the atoms are confined within a paraboloid of equation:

$$x + \frac{\gamma}{2v^2}y^2 = \frac{v^2}{2\gamma}$$

whose summit is located at $\frac{v^2}{2\gamma}$ from the nucleus in the sunward direction. This paraboloid is a surface of discontinuity for the intensity in this monocinetic model. Such a discontinuity is not observed and thus we look for a more realistic model allowing a velocity distribution $f(v)$ of ejected atoms centered around the mean velocity v_H (or flow velocity of H-atoms).

Model with Velocity Distribution $f(v)$

The hydrogen envelope can be thought of as a collisionless expanding atmosphere surrounding a small region of radius r_c, inside which collisions are frequent. When a H-atom is outside the sphere of radius r_c, two cases are possible according to the direction of its velocity: if the atom is directed toward the sphere of radius r_c, it will reenter it. If it is not, it will eventually cross a sphere radius $r_A > r_c$ large enough that its velocity can be considered as radial, but small enough that radiation pressure can be neglected. Then it is not necessary to consider the distribution of velocity directions, but only the distribution of velocity modules $f(v)$, which is conserved between r_c and r_A. Let n_A be the uniform density of atoms at r_A. The ejection rate per steradian $Q_W(v)\,dv$, or flux per second, per steradian, of atoms having a velocity between v and $v+dv$ and emerging from the inner region with radius r_A can be written:

$$Q_W(v)dv = dn_A r_A^2 v = n_A r_A^2 v f(v)dv.$$

If $v_H = \int_0^\infty v f(v)\,dv$ is the mean velocity of the distribution $f(v)$ and Q_W the total flux per steradian, it can be easily demonstrated that:

$$Q_W(v)dv = \frac{Q_W}{v_H} v f(v)\,dv. \quad (8)$$

Replacing in (7) Q_W by $Q_W(v)dv$ and integrating over v we obtain the expression (9) of the density $n(r,\theta)$ when atoms are distributed at r_A according to the distribution $f(v)$:

$$n(r,\theta) = \frac{Q_W}{v_H}\int_0^\infty v f(v)(\phi_{\alpha_1}(r,\theta,v) + \phi_{\alpha_2}(r,\theta,v))\,dv. \quad (9)$$

Thermal Model

We call a thermal model a model in which all the hydrogen atoms are produced inside the region of radius r_c, where collisions are frequent enough that a kinetic temperature T can be defined. Then hydrogen atoms have a maxwellian distribution at distance r_c. The module part $f(v)$ of this distribution is conserved up to r_A:

$$f(v)dv = \frac{4}{\sqrt{\pi}}\frac{v^2}{v_W^3}\exp\left(-\left(\frac{v}{v_W}\right)^2\right)dv \qquad v \geqq 0 \quad (10)$$

where v_W is related to the temperature T by $v_W = \left(\frac{2kT}{m_H}\right)^{\frac{1}{2}}$. k is the Boltzmann's constant and m_H the mass of the H-atom. The mean velocity of this distribution is $v_H = \frac{2}{\sqrt{\pi}}v_W$. The shape of $f(v)$ is indicated in Fig. 26. Using Eq. (8), it is clear that, with the selected form of $f(v)$, the flux per steradian is then:

$$Q_W(v)dv = 2Q_W\frac{v^3}{v_W^4}\exp -\left(\left(\frac{v}{v_W}\right)^2\right)dv.$$

The density for the thermal model is then obtained by introducing in Eq. (9) the expression (10) of $f(v)$.

Lyman-Alpha Emission

The distribution of Lyman-Alpha emission emerging from a model was computed with the assumption that the hydrogen envelope was optically thin. This might not be true for a small region in the head of the comet, but comparisons with observations were restricted to the external region of the hydrogen cloud where the intensity was lower than 3 kilo Rayleigh, ensuring that the assumption is certainly acceptable. Furthermore, for comet Bennett it can be considered that the measured signal in this region was not perturbated by the convolution with the photometer F0V.

Lyman-Alpha intensity emerging from the hydrogen envelope is then proportional to the integrated number density N along the line of sight and to the flux F_0 at the center of the solar line:

$$I = \frac{g}{4\pi} N \text{ photons/cm}^2 \text{ s sterad}$$

where the excitation rate g at the distance R is related to the flux F_0 at $R_0 = 1$ AU by:

$$g = \frac{\pi e^2}{m_e c} f \cdot F_0 \left(\frac{R_0}{R}\right)^2$$

e and m_e are, respectively, the charge and the mass of the electron; f is the oscillator strength of the Lyman-Alpha transition, c is the velocity of light.

Comparison of the Thermal Model with Observations

The monocinetic model, confined inside a paraboloid, was rejected because it could not account for the large extension of the observed emission, though the fit for central isophotes was pretty good when the velocity was of the order of 7 to 9 km s^{-1}. Some dispersion had to be introduced with a velocity distribution $f(v)$. The thermal model has the great advantage to have a velocity distribution characterized by only one parameter. Furthermore it can be partly justified physically when one thinks that most of potential parent molecules which are candidates to produce, after photodissociation, usually observed components (CN, C_2, NH_2, OH ...), contain hydrogen and have a lifetime of the order of a few hours to thirty hours at 1 AU (Potter and Del Duca, 1964). In these conditions the hydrogen atoms would have a high probability to be produced inside the region of radius r_c where collisions are important. The shorter is the lifetime of parent molecules, the nearer from the nucleus the hydrogen atoms are produced.

Besides these physical assumptions, it was decided to compare our observations to the thermal model mostly because its velocity distribution depends upon a single parameter (T, v_W or v_H). The intensity distribution of the thermal model depends then upon three parameters: the ejection rate Q_W at the time of observation, the mean ejection velocity v_H of atoms, and their lifetime τ_H. This later parameter is not completely unknown, since we have an estimate of the charge-exchange process and photo-ionization at 1 AU:

Photo-ionization rate $J = 0.70 \times 10^{-7}\ s^{-1}$,

Charge-exchange cross-section $\sigma_{ex} = 2 \times 10^{-15}$ cm^2

Flux of solar protons $\phi_p = 1.5 \times 10^8$ proton/cm^2 s.

J was deduced from the EUV solar spectrum of Hall and Hinteregger (1970) and from theoretical photo-ionization cross sections of Bethe and Salpeter (1957). The protons flux ϕ_p was estimated for the ecliptic longitude of comet Bennett by Collard and Wolfe (1972), from the Pioneer-9 data and a corotation calculation. The corotation delay was found to vary from -9 to -12 days between the 1st and the 30th of April, 1970. The use of the corotation delay is based upon the assumption that the solar activity of a certain solar region remains steady.

These values yield a mean lifetime τ_H before ionization for an H-atom at one AU:

$$\tau_H(1\text{ AU}) = \frac{1}{\sigma_{ex}\phi_p + J} = 2.7 \times 10^6 \text{ s}.$$

However this value of τ_H holds for the ecliptic plane only, whereas the ecliptic latitude of the comet changed from 30° to 80° during the observations. Should the flux of solar wind protons be different outside the ecliptic plane, τ_H would also be different. For this reason this parameter was let free in our data analysis, in order to detect any possible change with the ecliptic latitude.

In order to determine the three parameters v_W, Q_W, τ_H corresponding to one intensity map, we compared the measured and computed distributions of intensities along three lines indicated in Figs. 6 and 18:

– The forward and the backward profiles, along NX' and NX'' respectively.

– One perpendicular profile (parallel to NY), cutting NX'' at 10^6 km behind the nucleus (Fig. 6).

We first remark that Q_W is a multiplicative factor for the three profiles. Using various values of the parameters, it was found that the computed intensity distributions reacted differently to the parameters according to the type of profile. The slope of the backward profile was only sensitive to τ_H (the time of flight of one atom in the background part of the comet is of the order of τ_H), and, to a much lesser extent, sensitive to v_W. Then the lifetime was determined by comparing the slopes of computed and measured backward profiles (Fig. 19a). The slope of the forward profile was found to be mainly sensitive to the velocity v_W. Physically, this clearly makes sense since the atoms going forward have to fight against the Lyman-Alpha radiation pressure; the larger their velocity, the further they go, but in any case they spend in the forward part of the envelope a time smaller than τ_H. Once τ_H was determined with the backward profile, the velocity v_W was determined with the slope of the measured forward profile (Fig. 19b). It was checked that an error of τ_H by a factor 2 was not changing v_W by more than 1 km s^{-1}.

Introducing these values of τ_H and v_W in the model with an arbitrary value Q_W^0 of the production rate, we compared simultaneously the backward and the forward

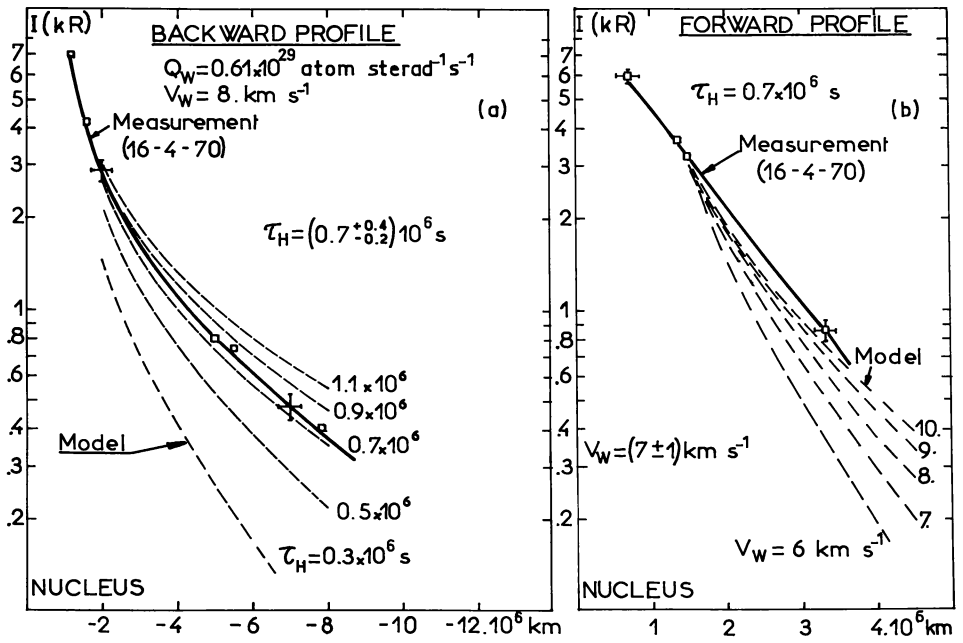

Fig. 19a. Comparison of measured and computed intensity distributions along the backward profile for various values of the lifetime τ_H. The slope of the observed distribution corresponds to $\tau_H = 0.7 \cdot 10^6$ s

Fig. 19b. The slope of the computed forward profile depends essentially on the ejection velocity. They were normalized at 3 kR at $1.5 \cdot 10^6$ km in front of the nucleus

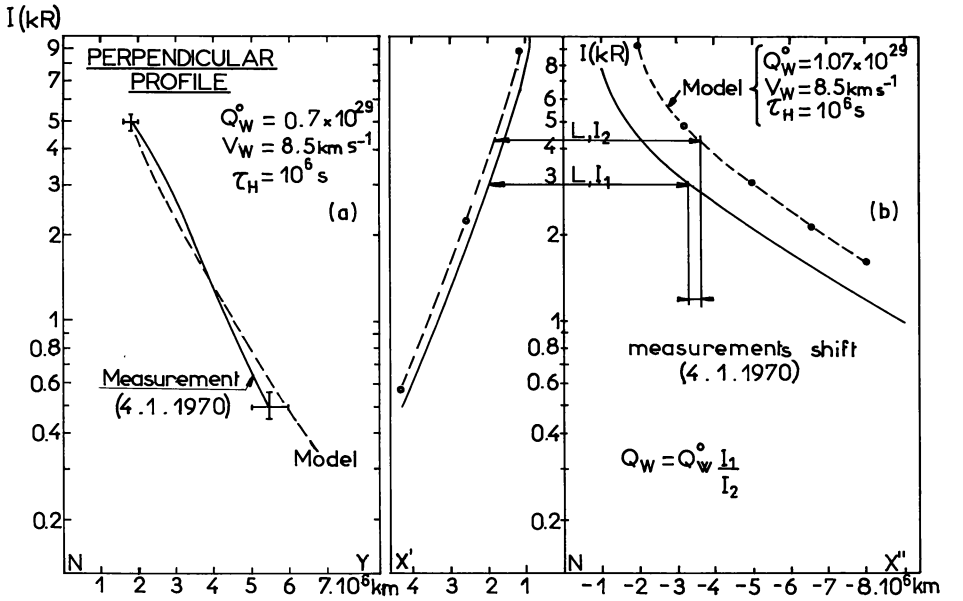

Fig. 20a. Once the slopes of the backward and forward profiles have been adjusted, the model curve can be superimposed on the measured curve by a mere translation. The vertical translation provides the production rate, the horizontal translation provides the position of the nucleus of the model relative to the measured profile

Fig. 20b. The comparison of perpendicular profile is used as a global check of the three parameters v_W, Q_W, τ_H

profiles (Fig. 20a). As the slopes were already adjusted, only one translation was necessary to superimpose the measured profile $X'X''$ to the computed profile. The vertical component of this translation was the ratio Q^0_W/Q_W, while the horizontal component allowed to determine the exact location of the nucleus along the measured profile, as it is indicated by the letter N in Figs. 6–16.

It was checked that the set of parameters thus determined provided also a satisfactory fit for the perpendicular profile $N\,Y$ (Fig. 20b), indicating that the general shape of the isophotes was well represented by the thermal

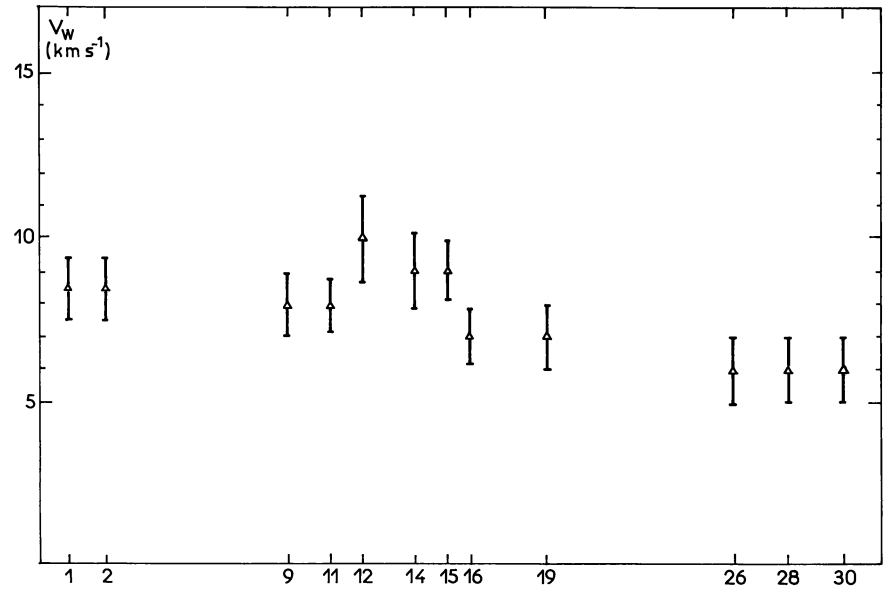

Fig. 21. Variation of the ejection velocity v_W along the month of April, 1970, as determined with forward and perpendicular profiles. The error bars reflect the instrumental error and allows for a possible variation of $\pm 50\%$ of the lifetime of a hydrogen atom. Though the sun-comet distance increased from 0.61 to 1.1 AU v_W did not change significantly

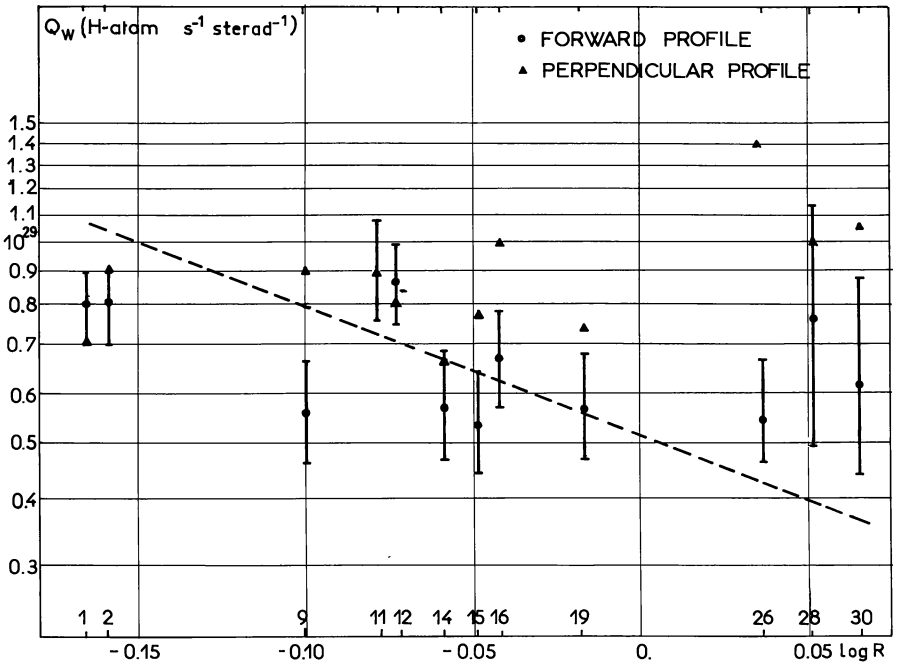

Fig. 22. Variation of the H-atoms ejection rate Q_W (number of atoms produced per second and per steradian) as a function of heliocentric distance R. Perpendicular and forward profiles yield similar values of Q_W, indicating an isotropic production rate. The variation of Q_W follows approximately a R^{-2} law (dashed line), except for the last three maps for which Q_W seems higher

model. The values of the parameters determined for the different maps are presented in Figs. 21, 22 and 23. The thermal ejection velocity v_W is plotted as a function of time (Fig. 21). The ejection rate Q_W is plotted as a function of log R (Fig. 22) along with a R^{-2} law. The lifetime reduced to $R_0 = 1$ AU, $\tau_H \times \left(\frac{R_0}{R}\right)^2$, is presented as a function of heliographic latitude (Fig. 23), together with the solar wind protons flux which yields this lifetime, assuming that the photo-ionization rate J is isotropic and constant in time.

In the next section, we discuss the compatibility of these results with the hypothesis that the parent molecule would be water.

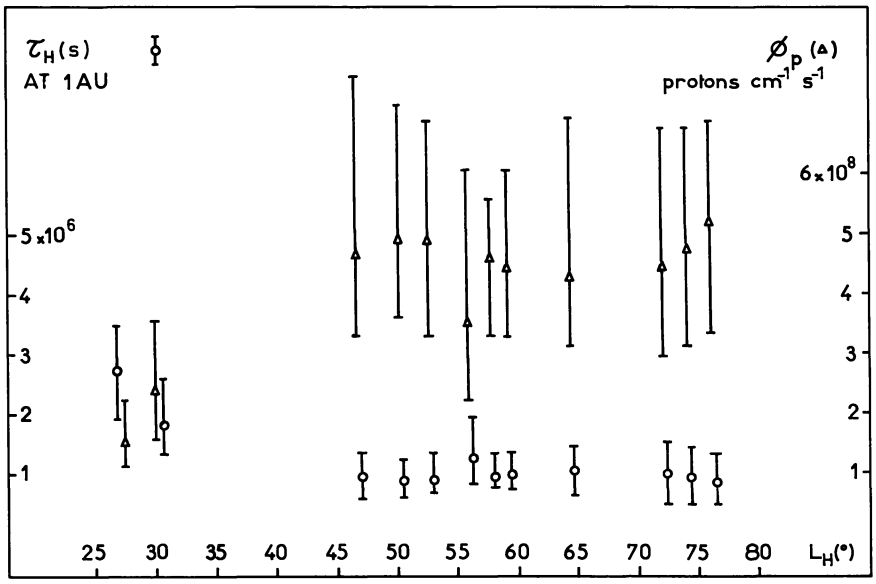

Fig. 23. The lifetime τ_H reduced to one AU is plotted versus the heliographic latitude L_H, together with the corresponding solar wind protons flux if the EUV solar flux is assumed to be constant. The data suggest an increase of a factor of 3 in the protons flux above $L_H \simeq 45°$

Discussion

Ejection Velocity

Mendis *et al.* (1972) have recently given a hydrodynamic description of a cometary atmosphere composed of H_2O and its daughter products OH, H and O, coupled through frictional interaction, up to a radial distance of 10^6 km from the nucleus. However, collisions are already negligible at a radial distance of 10^5 km, and an exospheric description would be more appropriate to describe the outer regions of the hydrogen envelope ($r > 10^6$ km). Nevertheless, they proved that the Lyman-Alpha emerging from the optically thick central region was a function of the temperature alone and was not dependent upon the production rate of hydrogen atoms. From the intensity of 42 kR observed in the 1′ field of view of the OAO–2 instrument, near the center of comet Bennett, they derived a temperature of the coma of 3000 °K.

The variance of the ejection velocity v_W during the month of April was small, and its mean value, 8 ± 2 km s^{-1}, corresponds to a kinetic temperature $T = (3900 \pm \frac{2100}{1700})$°K. This temperature is slightly larger than the value of 3000 °K derived by Mendis *et al.* (1972). In fact, even the validity of a thermal model appears questionable. However, any other model which might be sought to fit the data must have a flow velocity

$$v_H = \frac{2}{\sqrt{\pi}} v_W \simeq 9 \text{ km s}^{-1},$$

and some scattering in its velocity distribution, because these two features derived from the data analysis are not model dependent.

Instead of having a thermal origin, the velocity of an H-atom may be the result of the energy budget of the photo-dissociation process of the parent molecule MH, if it occurs in a region where collisions are negligible.

$MH + h\nu \rightarrow M + H +$ kinetic energy.

The model of a nucleus having an ice core from which H_2O is vaporized and then photo-dissociated by the solar flux is somewhat supported by the OAO–2 observation of a strong OH emission around 3090 Å, in comet Bennett, though Wallis (1972) pointed out that the reported variation of OH emission did not support completely the evaporating icy model.

Since water is one of the most likely candidate as a parent molecule, according to Whipple (1950) and OAO observations, we have focused our attention on this molecule. First we examined how the excess energy $\Delta E = h\nu - h\nu_g$ is distributed ($\lambda_g = 2420$ Å is the wavelength upper limit of H_2O photo-dissociation). But before dissociation, H_2O goes through a pre-dissociation state whose energy requires photons of wavelength $\lambda < 1860$ Å. Taking the solar spectrum of Thekackara (1970) and Widing *et al.* (1970), and the absorption cross section of water vapor as a function of wavelength (Watanabe *et al.*, 1953), the lifetime of H_2O at 1 AU is estimated to be ≈ 30 h. If 1357 Å $< \lambda <$ 1860 Å, OH is produced in the ($^2\pi$) state, and most of the excess energy goes to the H-atom as kinetic energy. In this case the distribution of ΔE has approximately a gaussian shape centered at 2 eV with a half width of 0.9 eV at 1/e. This excess energy corresponds to a mean velocity of the H-atom of 19 km s^{-1}. On the contrary, if $\lambda < 1357$ Å, OH is produced in the excited state ($^2\Sigma^+$), and the excess energy received by the H-atom lies between 0.1 and 1.1 eV (Tucker Carrington, 1964) corresponding to a velocity between 4 and 12 km s^{-1}. The ratio of fast atoms to slower atoms is computed to be 0.9.

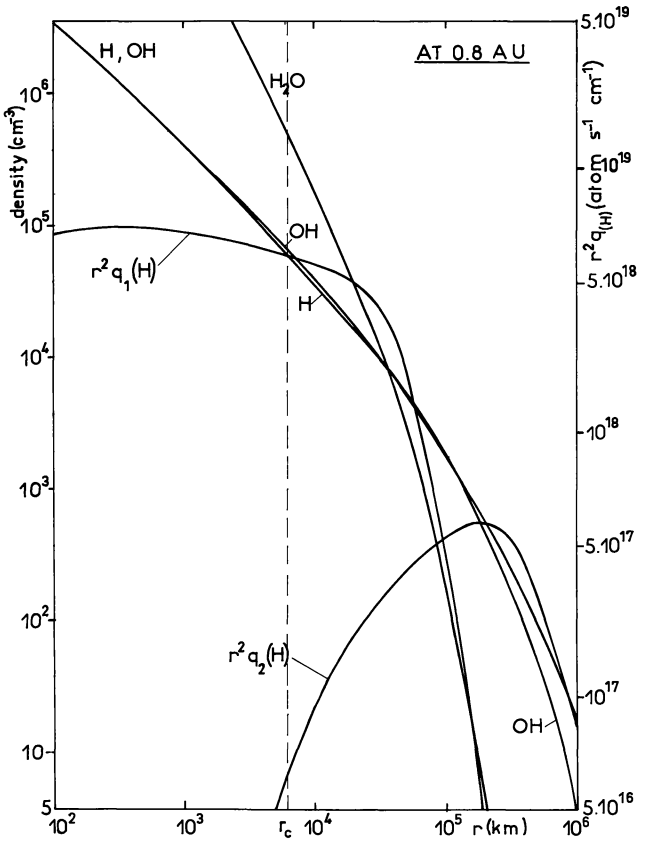

Fig. 24. The distribution density of H, OH and H_2O as a function of distance to center of comet r is taken from the water model of Mendis *et al.* (1972), after adjustment of the production rate of atoms to our observed value. The production rates per unit length of $r\,r^2q_1(H)$ and $r^2q_2(H)$ are also indicated respectively for the photo-dissociation of H and the photo-dissociation of OH. All OH and 80% of H_2O are photo-dissociated outside the sphere of critical radius r_c, where there is no more collisions

Little is known about the photo-dissociation of OH and the resulting excess energy; however it can be estimated to be 0.1 – 0.4 eV, leaving the H-atom with a velocity of 4 to 8 km s^{-1}.

In order to analyze further the hypothesis of water as the only parent molecule, we have to know whether the H-atoms are produced in the thermalized region of the comet ($r < r_c$) or in the region where collisions are negligible ($r > r_c$). From the study of the hydrodynamic model of Mendis *et al.*, it is possible to define the critical radius r_c as the distance from the nucleus at which an H-atom with an outward velocity has a probability e^{-1} to escape without suffering any further collision with H_2O or OH. Adjusting their production rate to the value that we found for comet Bennett on April 16, 1970, ($Q_W = 0.7 \times 10^{29}$ H-atom sterad^{-1} s^{-1}, we found $r_c = 8 \times 10^3$ km, with a density of

$$1.25 \times 10^{12} \text{ atom cm}^{-3}$$

and a flow velocity $U_0(H_2O) = 0.3$ km s^{-1} at $r_0 = 10$ km from the center.

From the density distributions of H_2O and OH and their photo-dissociation rates given by Mendis *et al.*, we have computed the production rates per unit length and per steradian $r^2q_1(H)$ and $r^2q_2(H)$ as a function of r (Fig. 24). Neglecting the attenuation of the solar flux, they are:

$$r^2q_1(H) = r^2 \times 1.6 \times 10^{-5} R^{-2} n(H_2O),$$
$$r^2q_2(H) = r^2 \times 1.4 \times 10^{-6} R^{-2} n(OH).$$

It is found that all hydrogen atoms coming from the photo-dissociation of OH are produced outside the sphere of radius r_c, in the collisionless region. The ratio Q_1/Q_1' of H-atoms generated from the first photo-dissociation of water inside and outside the sphere of radius r_c is:

$$\frac{Q_1}{Q_1'} = \frac{\int_{r_0}^{r_c} r^2 q_1(H)\,dr}{\int_{r_c}^{\infty} r^2 q_1(H)\,dr} \simeq 0.2$$

In this pure water model we can then distinguish four kinds of H-atoms according to their parent (H_2O or OH), their production zone and their velocity distribution. The characteristics of these four components and their corresponding production rates relative to Q_W are summarized in Table 1.

There is some degree of flexibility in this model since the velocity distributions of components 1 and 2 are not known. We have explored the influence of the mean velocity of component 1, since it has the higher weight, keeping fixed the velocity distribution of component 2 as a gaussian distribution with a mean velocity of

Table 1

Component	Parent molecule	Production zone	Velocity distribution (km s^{-1})	Production rate
1	$OH(^2\pi) + h\nu_1 \rightarrow H + O(^3P)$	$r > r_c$	$4 < v < 8$	$0.5\,Q_W$
2	$H_2O + h\nu_2 \rightarrow H + OH(^2\Sigma^+)$	$r > r_c$	$4 < v < 12$	$0.2\,Q_W$
3	$H_2O + h\nu_3 \rightarrow H + OH(^2\pi)$	$r > r_c$	$v = 19 \pm 2$	$0.2\,Q_W$
4	$H_2O + h\nu_3 \rightarrow H + OH(^2\pi)$ $H_2O + h\nu_2 \rightarrow H + OH(^2\Sigma^+)$	$r < r_c$	Thermalized $v_W = 8$	$0.1\,Q_W$

$\lambda_1 = c/\nu_1 < 2820$ Å; $\lambda_2 < 1357$ Å; 1357 Å $< \lambda_3 < 1860$ Å.

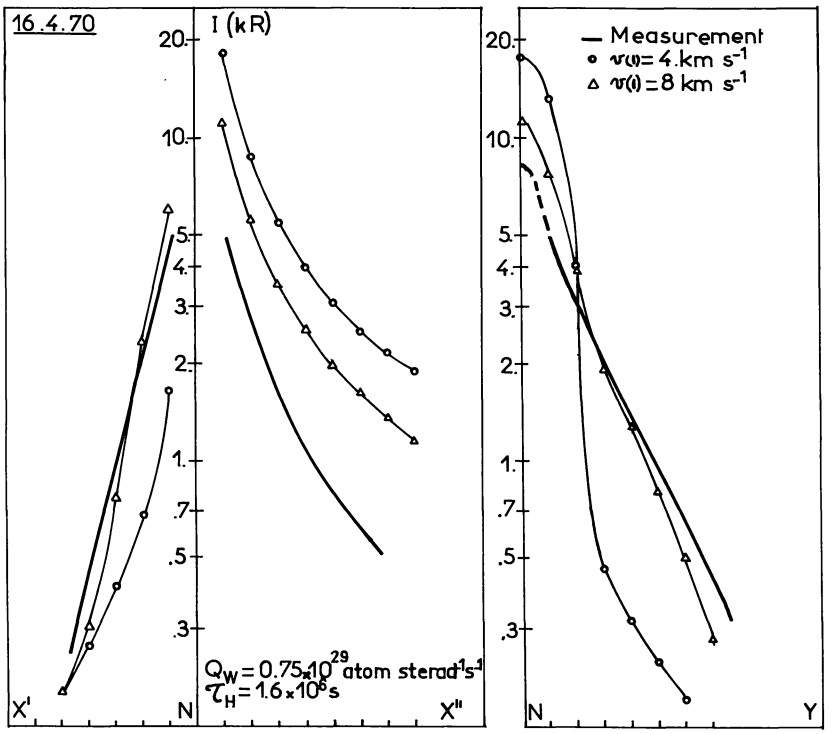

Fig. 25. Comparison of observed intensity distributions along $X'X''$ and NY for April 16, 1970 with the computed intensity distribution in a pure water model. Two velocity distributions $v(1)$ are considered for H-atoms produced from OH, the most important of the four components. The slow velocity distribution is not compatible with observations (perpendicular profile)

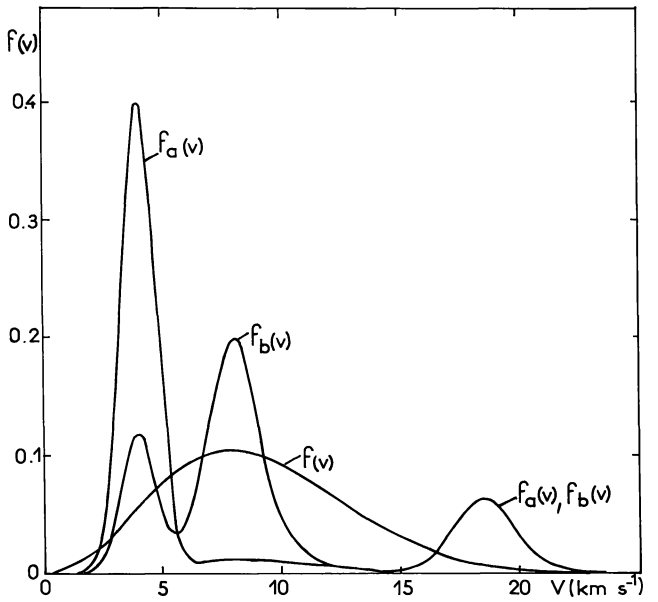

Fig. 26. The distributions $f_a(v)$ and $f_b(v)$ result from the addition of the four components of a pure water model in two different cases, with the velocity of component 1 centered either at 4 km s^{-1} or at 8 km s^{-1} respectively. The distribution $f(v)$ is the maxwellian velocity distribution of the thermal model with a thermal velocity $v_W = 8$ km s^{-1}, which can be considered as a rough approximation of $f_b(v)$

4 km s^{-1} and a dispersion of ± 1 km s^{-1}. Together with the data obtained for April 16, 1970, the intensity distributions along $X'X''$ and NY which would result from such a model is shown by dashed lines in Fig. 25 for two gaussian velocity distributions of component 1:

a) $v = 4 \pm 1$ km s^{-1}.

b) $v = 8 \pm 1.5$ km s^{-1}.

The velocity distributions of the cumulated components with their own weights are indicated in Fig. 26 as $f_a(v)$ and $f_b(v)$ for cases a and b respectively. Several features can be pointed out:

– the computed perpendicular profile is in disagreement with the observations for case a), ruling out a slow velocity distribution for the H-atoms coming from the OH photodissociation.

– the case b) is in good agreement with observations both for the perpendicular and the forward profiles. The discrepancy for the backward profile can be reduced by taking a smaller lifetime τ_H, in accordance with the lifetime derived from the comparison of observations with the thermal model, without changing the two other profiles. The good fit for the forward profile indicates that the data are compatible with the existence of the fast atoms of component 3, because the weight of this component is only 20%.

The main conclusion of our analysis is that the velocity of the hydrogen atoms is extremely dependent on the $OH + h\nu \rightarrow O + H$ reaction. In the absence of any experimental data on the photo-dissociation rates for this reaction, and since we can make a choice of the corresponding velocity between 4 and 8 km s^{-1}, our

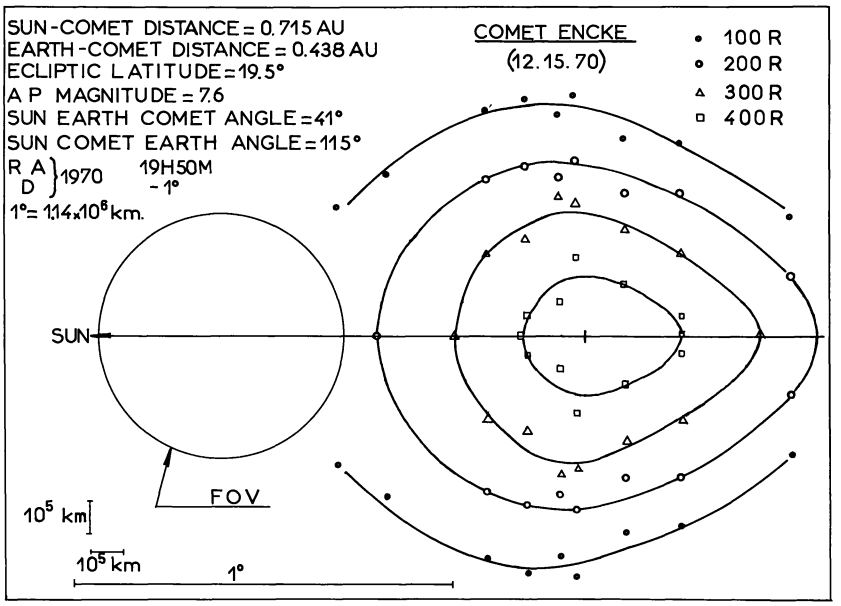

Fig. 27. Isophotes of Lyman-Alpha emission of comet Encke, observed in December 1970. The field of view of the instrument covered a large part of the comet, and the map is the convolution of the emission by the field of view. The emission was much weaker than for comet Bennett; the production rate was found to be $Q_W = 5 \times 10^{26}$ atom/s steradian

observations are compatible with a pure water model. Measurements of the photodissociation rates of OH and wavelength dependence are sorely needed to solve the problem; if they would demonstrate that the value of v would be significantly different than 8 km s^{-1}, other constituents than H_2O would have to be considered.

Production Rate of H-*atoms*

Two determinations of the production rate Q_W are indicated as a function of log R in Fig. 22: one derived from the backward and forward profiles, the other from the perpendicular profile. Apart from the three values obtained at the end of April, they are not essentially different from one another, and seem to follow approximately a R^{-2} law. It is important to point out that this conclusion is independent of our *a priori* assumption that such a R^{-2} law was followed; in a first analysis for which we assumed that the production rate had remained constant up to the moment of observation, such a law had already been found, suggesting performing a first order correction as described above.

The value of $Q_W = 0.7 \times 10^{29}$ atom sterad^{-1} s^{-1} found for April 16, 1970, was compared to the value of $0.65 \cdot 10^{29}$ atom sterad^{-1} s^{-1} derived by Keller (1971a) from essentially the same data, but with a somewhat different approach. After a careful analysis in common of all the detailed calculations in both cases, we found several minor differences which could account for the discrepancy. It was concluded that our value was correct within $\pm 30\%$, this uncertainty reflecting mainly the uncertainty on the solar Lyman-Alpha flux.

Keller (1971b) examined the OAO–2 observations, namely a map of the intensity in a region with a radius of 10^6 km from the center, obtained on 16.4.1970. From the central intensity, 42 kR, and the intensity decrease with radial distance, Keller derived a total production rate $Q_t = 3.2 \times 10^{30}$ H-atom s^{-1} and a mean velocity $v_H = 7$ km s^{-1} (1973).

Lifetime of H-*atoms*

The lifetime of H-atoms (reduced to 1. AU), as deduced from the comparison of data with the thermal model, is plotted as a function of heliographic latitude of comet Bennett (Fig. 23). There is a reduction of the lifetime by a factor of $\simeq 2$ between 31 and 47° of latitude. If we assume that ionization by the solar EUV flux does not depend upon the heliographic latitude, the variation of the lifetime could be attributed to a larger ionization by the solar wind protons by a factor of $\simeq 3$. Indeed, a noticeable increase in the solar wind velocity at high latitudes was measured (Coles and Maagoe, 1972) by using interplanetary scintillation of radio sources. However, the density would also have to be increased by a small factor to explain this larger ionization.

Observation of Comet Encke (1970e)

Comet Encke was observed on December 12, 1970, with the same instrument. Its Lyman-Alpha emission, although much fainter than for comet Bennett, could be clearly identified. Iso-intensity contours were determined (Fig. 27) but the spatial resolution of the instrument was not good enough to perform a detailed comparison with

the model. The size of the envelope was an order of magnitude less than the size of comet Bennett. Then the time of flight of a H-atom was much shorter than its lifetime, and this parameter could not be determined.
The thermal model was applied, taking into account the convolution of intensity by the FOV of the instrument. The fit with observations was found to be unsensitive to the velocity distribution and to the thermal velocity v_W. The production rate Q_W was found to depend upon the assumed value of v_W:

if $v_W = 7\ \mathrm{km\ s^{-1}}$, $Q_W = 4.5 \times 10^{26}$ atom sterad^{-1} s^{-1},
if $v_W = 10\ \mathrm{km\ s^{-1}}$, $Q_W = 6 \times 10^{26}$ atom sterad^{-1} s^{-1}

that is to say approximately two orders of magnitude lower than the production rate of comet Bennett at the same distance to the sun (April 9, 1970) whereas the difference of visual magnitudes was 5.8, corresponding to a brightness ratio of 200.
During May 1971, a similar search for a Lyman-Alpha emission was performed on comet Toba, then of magnitude 8.1. No Lyman-Alpha emission could be detected from comet Toba, notwithstanding the fact that its magnitude was essentially similar to the magnitude of comet Encke. This would place an upper limit on the production rate of $Q \simeq 2 \times 10^{26}$ atom/s steradian for comet Toba.

Conclusion

A series of Lyman-Alpha isophotes of comets Bennett and Encke have been obtained and analyzed.
1. The data provide values of the ejection velocity v_W, the production rate Q_W and the ionization lifetime τ_H of H-atoms. The typical values are:

$v_W \simeq 8.0 \pm 1\ \mathrm{km\ s^{-1}}$
$Q_W = 0.7 \times 10^{29}$ atom sterad^{-1} s^{-1} for comet Bennett
$Q_W \simeq 5 \times 10^{26}$ atom sterad^{-1} s^{-1} for comet Encke
τ_H at 1 AU: $2 \cdot 10^6$ s for heliographic latitudes up to 30°, and $\simeq 10^6$ s for heliographic latitudes larger than 45°.

2. Since, in a pure H_2O model, most of observed atoms would originate outside the thermalized region, the ejection velocity would be only related to the energy budget of the photo-dissociation reaction. In the absence of data about photo-dissociation of OH, the value of 8 km s^{-1} is compatible with a pure H_2O parent molecule.
3. There is a strong indication for a fast increase of the solar wind flux around 30 to 45° of heliographic latitude.

Acknowledgements. It is a pleasure to acknowledge our debt to M. Dubin at NASA Headquarters, to E. Mercanti at the OGO Project Office and to the OGO Control Center Staff. We have to congratulate specially W. Fritts who conducted the spacecraft and experiment operations during the month of April, 1970.
We wish to thank Dr. Keller for very useful discussions and Dr. Philippe Lamy for the revision of manuscript. Data reduction and model calculations were performed at the Centre de Calcul de l'INAG, Observatoire de Meudon.
This work was supported under CNES contracts: 66 CNES 003, 66 CNES 011, 67 CNES 201, 68 CNES 202, 69 CNES 225, 70 CNES 299, and 71 CNES 201.

References

Bethe, H., Salpeter, E. 1957, Handbuch der Physik, Ed. S. Flügge. Springer, Berlin, Göttingen, Heidelberg, p. 389, 390.
Bertaux, J. L., Blamont, J. E. 1971, *Astron. & Astrophys.* **11**, 200–217.
Bertaux, J. L., Blamont, J. E. 1970, *Compt. Rend. Acad. Sci. Paris* **270**, 1581.
Biermann, L. 1968, Jila report 93.
Biermann, L., Trefftz, E. 1964, *Z. Astrophys.* **59**.
Carrington, T. 1964, *J. Chem. Phys.* **41**, 7, 2012–2018.
Code, A. D., Houck, T. E., Lillie, C. F. 1970, I.A.U. Circular n° 2201.
Coles, W. A., Maagoe, S. 1972, *J. Geophys. Res.* **77**, 5622.
Hall, L. A., Hinteregger, H. E. 1970, *J. Geophys. Res.* **75**, 34.
Haser, L. 1965, *Coll. l'Univ. Liège* **37**, 233.
Jenkins, E. B., Wingert, D. W. 1972, *Astrophys. J.* **174**, 697.
Keller, H. U. 1971a, *Mitt. Astron. Ges.* **30**, 143–148.
Keller, H. U. 1971b, Inaugural Dissertation zur Erlangung der Doktorwürde, Fakultät der L. Maximilians Universität, München.
Keller, H. U. 1973, *Astron. & Astrophys.* **23**, 269.
Mendis, D. A., Holzer, T. E., Axford, W. I. 1972, *Astrophys. Space Sci.* **15**, 313.
Potter, A. E., Del Duca, B. 1964, *Icarus* **3**, 103.
Thekackara, M. P., 1970, *J. Environmental Sciences*, Sept./Oct.
Thomas, G. E. 1973, Private communication.
Vidal-Madjar, A., Blamont, J. E., Phissamay, B. 1973, to be published in *J. Geophys. Res.*
Wallis, M. K. 1972, *Science* **178**, 78.
Watanabe, K., Zelikoff, M., Inn, E. C. Y. 1953, AFCRL Tech. Rept. **52**, 23.
Whipple, F. 1950, *Astrophys. J.* **111**, 375.
Widing, K. G., Purcell, S. D., Sandlin, G. D. 1970, *Solar Phys.* **12**, 52.
Wolfe, J., Collard, R., 1972, Private communication.

J. L. Bertaux
J. E. Blamont
M. Festou
Service d'Aéronomie du C.N.R.S.
F-91370 Verrières-le-Buisson, France